AIP Journal of Applied Physics

Dual band complementary metamaterial absorber in near infrared region

Prakash Pitchappa, Chong Pei Ho, Piotr Kropelnicki, Navab Singh, Dim-Lee Kwong, and Chengkuo Lee

Citation: Journal of Applied Physics **115**, 193109 (2014); doi: 10.1063/1.4878459
View online: http://dx.doi.org/10.1063/1.4878459
View Table of Contents: http://scitation.aip.org/content/aip/journal/jap/115/19?ver=pdfcov
Published by the AIP Publishing

JOURNAL OF APPLIED PHYSICS **115**, 193109 (2014)

Dual band complementary metamaterial absorber in near infrared region

Prakash Pitchappa,[1,2] Chong Pei Ho,[1,2] Piotr Kropelnicki,[2,a)] Navab Singh,[2]
Dim-Lee Kwong,[2] and Chengkuo Lee[1,b)]
[1]*Department of Electrical and Computer Engineering, National University of Singapore, 4 Engineering Drive 3, Singapore 117576*
[2]*Institute of Microelectronics, A*STAR (Agency for Science, Technology and Research), 11 Science Park Road, Science Park II, Singapore 117685*

(Received 6 January 2014; accepted 6 May 2014; published online 21 May 2014)

In this paper, we present the dual band absorption characteristics of complementary metamaterial absorber in near infrared (1.3–2.5 μm) region. The dual band absorption is caused by two distinct resonance mechanisms—electrical resonance and cavity resonance. Electrical resonance occurs in the metal layer—top complementary metamaterial and the cavity resonance occurs in the spacer cavity formed between the top complementary metamaterial and bottom metal reflector layers. In order to elucidate the resonant mechanisms and study the effects of geometrical variations on both the resonant absorption behaviours, two sets of experiment were performed. It was seen that with increasing complementary metamaterial pattern dimension, the electrical resonance absorption peak showed a blue shift, while the cavity resonance showed a slight red shift. However, on the other hand, for the increase in spacer thickness, the cavity resonance peak showed a strong red shift, while the electrical resonance peak remained uninfluenced. The reason for these geometrical dependencies, for both resonances, is conceptually analysed. Furthermore, the design was optimized to attain single absorption band by engineering the cavity and electrical resonances to be at the same wavelength. The single absorption band was successfully realized, however, the peak wavelength showed a red shift from the electrical resonance as in dual band absorber case. The reason for the shift was further explored to be caused due to the strong coupling of electrical and cavity resonances. This approach of utilizing different resonant mechanisms for absorption at different wavelengths provides the means to achieve multiband absorbers, using a simple design and low cost fabrication process. © *2014 AIP Publishing LLC*. [http://dx.doi.org/10.1063/1.4878459]

I. INTRODUCTION

Electromagnetic metamaterial is an array of subwavelength structures which can be engineered to achieve specific material properties that do not occur in nature like negative permittivity, negative permeability, negative refractive index, etc. With the experimental demonstration of negative refractive index by Smith *et al.*,[1] there has been an extensive study on various design and functionality of metamaterial for a wide range of applications like invisibility cloaking,[2,3] sub-diffraction imaging,[4–7] perfect electromagnetic absorbers,[8–12] optical black hole,[13,14] wavelength selective blackbody emitters,[15–17] and many more. The metamaterial absorber has become a popular topic, since its first report by Landy *et al.* in 2008, as the proposed absorber was extremely thin and provided design flexibility to achieve close to perfect absorption at desired frequency, over a wide range of electromagnetic spectrum from microwave,[8] terahertz (THz),[9,57–60] infrared (IR)[10] to visible frequencies.[11]

Metamaterial absorbers in microwave and THz region have been extensively studied due to large feature size of single unit cell that are easier to be fabricated, compared to that in IR or visible frequency range. Even though, the extremely small feature size of IR metamaterial demands for a high control in fabrication, due to the increasing interest in the use of IR metamaterial absorbers in a number of applications like IR detectors,[18–22] solar cells,[23–25] chemical sensing,[26–28] etc., perfect metamaterial IR absorbers are been actively researched in recent times.[10,29–41] Most of the designs for IR perfect absorbers adopt the conventional trilayer absorber structure with top structured metamaterial layer, middle dielectric spacer layer, and bottom metal reflector. Usually, for IR absorption, plasmonic or electrical resonance in the top metal nanostructures are used.[10,29,37,55] Dual and multiband absorption in IR region are also designed using the plasmonic or electrical resonances, either through two or more metamaterial structures in a single unit cell,[37–39] or through single metamaterial pattern with split symmetry with respect to the polarization of incident light.[29] Dual band absorption is also reported by using two different dielectric spacer materials,[40] or different thickness of same dielectric material in a single absorber unit cell.[25] The multiple dielectric material or thickness based dual band absorbers majorly traps the magnetic component of the incident electromagnetic wave. In all the above cases, the structures are more complex to design and fabricate as they have multiple layers or use exotic materials. Simpler devices like single metamaterial pattern with split symmetry are polarization sensitive and hinder their use in real practical applications. Most of the reported metamaterial IR absorbers use either gold or silver as their structural layer material and electron beam lithography,

[a)]Currently affiliated with Excelitas Technologies, 8 Tractor Road, Singapore 627969
[b)]Author to whom correspondence should be addressed. Electronic mail: elelc@nus.edu.sg

self-assembly or focused ion beam for fabrication process. Neither of these materials nor fabrication processes is complementary metal oxide semiconductor (CMOS) compatible. Demonstration of device fabrication with CMOS compatible process and materials is a key milestone towards commercialization of this technology.

In this paper, we report a dual band near-IR (1.3–2.5 μm) absorber with complementary metamaterial (CMM) structure using CMOS compatible materials and processes. The CMM structure is a thin continuous metallic sheet with perforated holes etched into them.[42–44] Square hole patterns is used as the CMM shape for the proposed dual band absorber. The dual band absorption is obtained by exploiting the different resonant mechanisms—electrical and cavity resonances at different wavelengths. The conventional trilayer absorber structure with single top CMM unit cell layer and bottom reflector separated by a single spacer layer is used. The electrical resonance is caused due to the coupled mode excitation in the top nanostructured CMM layer and the bottom Mo reflector layer, while the cavity resonance is caused due to the dielectric spacer cavity formed between the CMM layer and bottom metal reflector. The dual band absorber device was engineered to achieve single band absorption by optimally designing the CMM pattern dimension and spacer thickness to excite both the electrical and cavity resonances at the same wavelength. Molybdenum (Mo) is used as the metal for top CMM and bottom reflector layers and Silicon di oxide (SiO_2) is used as the spacer dielectric material. Both Mo and SiO_2 are high temperature and radiation stable and are also CMOS compatible materials. Thus, the proposed absorber can be used in multi-colour infrared detection, gas sensing applications for rugged environments, and at a relatively low cost.[45,46]

II. UNIT CELL DEFINITION AND ITS ABSORPTION SPECTRUM

Fig. 1(a) shows the schematic representation of the unit cell of proposed CMM absorber that consists of top Mo CMM and bottom Mo reflector layers with SiO_2 spacer between them. The CMM design used is a continuous sheet of Mo layer with square holes etched in it. The periodicity of unit cell is given by "p" and the hole dimension of CMM is given by "a." The thickness of CMM (tm) and reflector (bm) layers is 100 nm and 200 nm, respectively, for all devices and are separated by a SiO_2 spacer layer of thickness of "d."

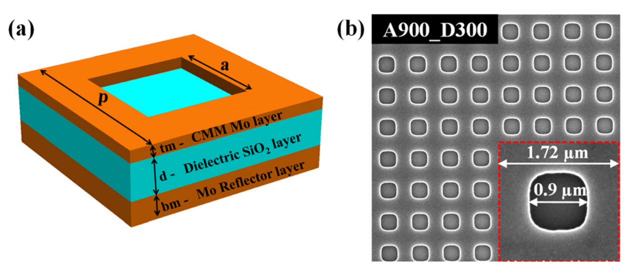

FIG. 1. (a) Schematics of dual band CMM absorber unit cell with period "p," hole dimension "a," and thickness of top CMM Mo, SiO_2 spacer and bottom Mo reflector layer as "tm," "d," and "bm," respectively. (b) SEM image of the fabricated absorber device with $p = 1.72\,\mu$m, $a = 900$ nm, $tm = 100$ nm, $d = 300$ nm, and $bm = 200$ nm. (Inset shows the fabricated unit cell of device A900_D300).

The device was fabricated using CMOS compatible process as described next. Bare 8 in. silicon wafer was cleaned and 200 nm of Mo was sputtered deposited, followed by plasma enhanced chemical vapour deposition (PECVD) of SiO_2. Then 100 nm thick Mo was deposited over the SiO_2 layer. Deep UV photolithography process was used to define the CMM square etch patterns. Finally, Mo was dry etched to form the final absorber structure. Fig. 1(b) shows the SEM image of fabricated absorber device with $p = 1.72\,\mu$m, $a = 900$ nm, $tm = 100$ nm, $d = 300$ nm, and $bm = 200$ nm and the inset shows the corresponding unit cell. The transmission and reflection measurement were carried out using a micro-photospectrometer operating in the near infrared region (1.3–2.5 μm). The transmission through the absorber sample was zero, $T(\lambda) = 0$ because of the bottom Mo perfect reflector, as the thickness of this Mo layer is much higher than the skin depth for incident IR wavelength range. The reflection spectrum, $R(\lambda)$ was measured with gold as reference, from which the absorption spectrum, $A(\lambda)$ is calculated as

$$A(\lambda) = 1 - R(\lambda) - T(\lambda), \qquad (1)$$

$$A(\lambda) = 1 - R(\lambda); \quad \text{as} \quad T(\lambda) = 0. \qquad (2)$$

From Eq. (2), we see that in order to maximize the absorption $A(\lambda)$ at desired wavelengths, the reflection $R(\lambda)$ must be suppressed at those wavelengths. The measured absorption spectra for the device A900_D300 is shown in Fig. 2, in which two distinct absorption peaks was observed and finite-difference time-domain (FDTD) simulations were performed to confirm the origin of these resonant absorption behaviours using Computer Simulation Technology (CST) software. The absorber structure is insensitive to polarization along x- and y-direction owing to the $\pi/2$ rotational symmetry along

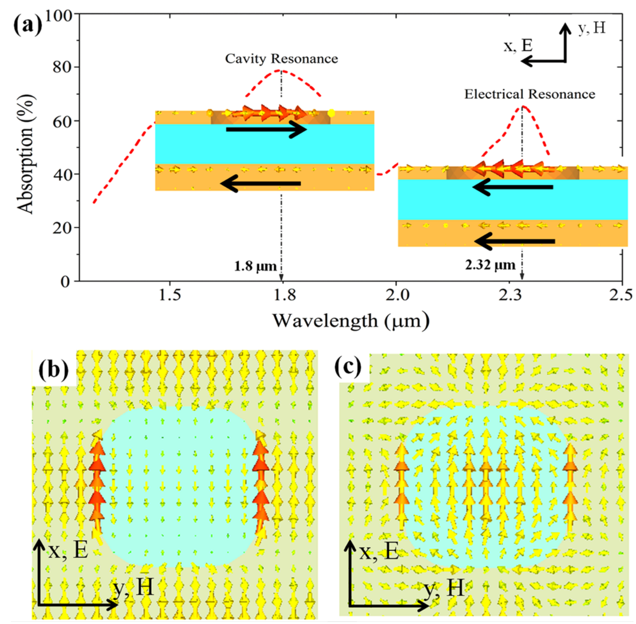

FIG. 2. (a) Measured absorption spectra of the A990_D300 sample and simulated surface current at $\lambda = 1.8\,\mu$m—Cavity resonance and $\lambda = 2.32\,\mu$m—Electrical resonance (Cross section along the E-k plane). (b) and (c) shows top view of the current distribution in the top CMM layer and bottom Mo reflector at cavity and electrical resonance, respectively.

z-direction at normal incidence.[47] The roundness of the CMM pattern corners were also included in the simulation model, with the radius of roundness value of 250 nm for A900_D300 device. For the FDTD simulation, the excitation source was incident with polarization of E field along x-direction. The permittivity of the lossless SiO_2 spacer was taken to be 2.1025,[48] and the permittivity of bulk Mo in the near-infrared was described by the Drude model with the plasma frequency, $\omega_p = 2\pi \times 1.81 \times 10^{15}$ rad s^{-1} and the damping constant, $\omega_c = 1.24 \times 10^{13}\, s^{-1}$.[49] The scattering parameters were simulated and the reflection coefficient was then calculated as $R(\lambda) = |S11(\lambda)|^2$. The measured absorption spectrum for A900_D300 with the simulated current density distribution at two peak absorption wavelengths at $\lambda = 1.8\,\mu m$ and $2.32\,\mu m$ at 45 incidence angle is shown in Fig. 2.[61] At $\lambda = 1.8\,\mu m$, the antiparallel currents in the top CMM and bottom reflector layers indicate a cavity mode resonance. At $\lambda = 2.32\,\mu m$, the majority of current is concentrated on the top CMM layer and a weak current in the bottom Mo layer, which indicates a coupled mode electrical resonance between the top CMM and bottom Mo layers.

III. STUDY ON GEOMETRICAL VARIATION

In order to further elucidate the dual absorption mechanisms due to the electrical resonance and cavity resonance, two set of experiments were carried out—one varying the CMM dimension (*a*) at fixed spacer thickness (*d*) and other by varying the spacer thickness (*d*) at fixed CMM pattern dimension (*a*). The results from these experiments are discussed in Subsections III A and III B.

A. Effect of CMM dimension (*a*)

To explore the effect of CMM dimension variation on the absorption peaks, three devices with varying CMM dimension, a = 900, 990, and 1080 nm and same spacer thickness, d = 300 nm were fabricated. Figs. 3(a)–3(c) show the SEM images of the fabricated devices with a = 900, 990, and 1080 nm, respectively (Inset shows the respective unit cell). The measured absorption spectra for the three devices are shown in Fig. 3(d). It can be seen that by increasing the CMM dimension the peak absorption wavelength due to electrical resonance shows a blue shift from 2.35 μm to 2.32 μm for the change of 0.18 μm in CMM dimension. In order to validate the effect of CMM dimension on peak absorption wavelength, a lumped equivalent circuit for the absorber device was formulated as shown in Fig. 4.[50–52] The resonant wavelength of the equivalent circuit can be written as below:

$$\lambda_{ER} = 2\pi C_0 \sqrt{(2L_1 + L_2)\left(\frac{2C_1C_2}{C_1 + 2C_2}\right)} \approx 2\pi C_0 \sqrt{(2L_1 + L_2)(C_1)}, \tag{3}$$

where C_0 is the speed of light in vacuum, $L_1 \sim \mu_r \cdot t_m \cdot (p - a)/(2a)$ is the inductance due to the CMM layer and μ_r is taken to be 1, L_2 is the inductance due to bottom continuous metal reflector, $C_1 \sim \varepsilon_0 \cdot t_m$ is the equivalent capacitance between the two opposite edges of the CMM pattern, and $C_2 \sim \varepsilon_0 \cdot \varepsilon_r \cdot (p - a) \cdot a/(2d)$ is the equivalent capacitance between the top and bottom metal layer. Since the majority of current is induced in the top CMM layer and the value of C_2 is much higher than C_1, the effective capacitance will be equal to C_1. Hence for simplicity, if the effect of bottom Mo reflector layer is neglected, the peak absorption wavelength due to electrical resonance can be written as, $\lambda_{ER} \sim 2\pi C_0(\varepsilon_r \cdot (p - a) \cdot t_m^{\,2}/2a)^{1/2}$.

It can be seen that the increase in CMM dimension (*a*) will reduce the value of λ_{ER} implying a shift to lower wavelength and explains the electrical resonance absorption peak shift in the measurement data shown in Fig. 3(d). On the

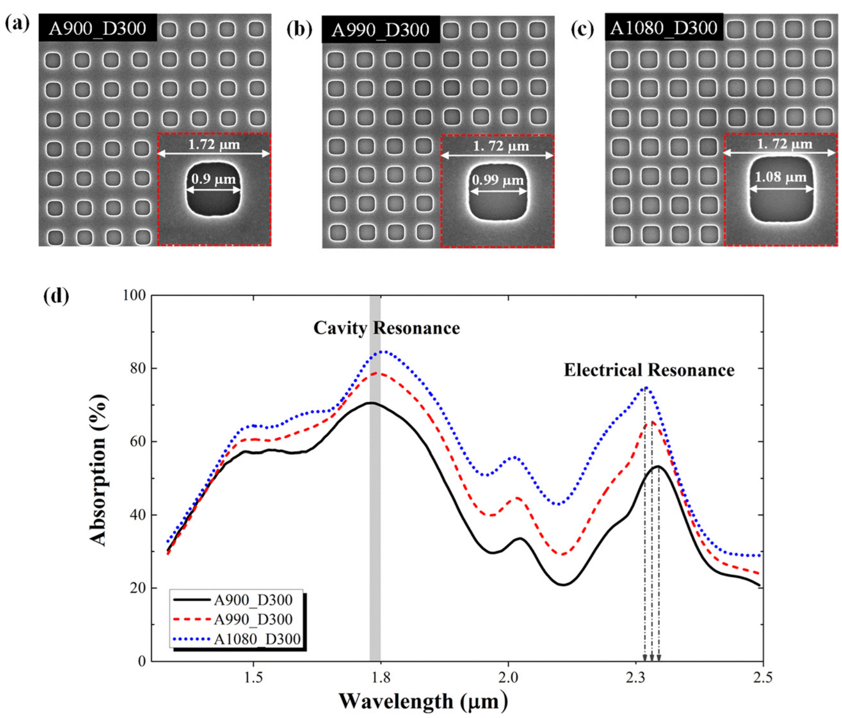

FIG. 3. SEM images of three fabricated devices with fixed spacer thickness, $d = 300$ nm and varying CMM dimension of (a) 900 nm, (b) 990 nm, and (c) 1080 nm, respectively (Inset: Zoomed in SEM image of respective unit cell). (d) Measured absorption spectra for the three devices - A900_D300 (Solid-Black), A990_D300 (Red-Dashed), and A1080_D300 (Blue-Dotted).

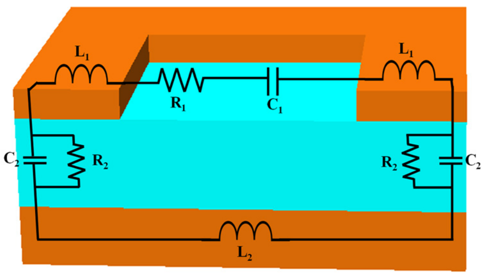

FIG. 4. Equivalent circuit for the complementary metamaterial absorber at electrical resonance.

other hand, the cavity resonant absorption peak for the three devices are around 1.78 μm which is shown as the shaded region in Fig. 3(d) and is blue shifted with increasing CMM dimension as well. This can be due to the increased phase shift caused due to the CMM dimension variation and so meagrely influences the cavity resonant peak. Additionally, the intensities of both electrical and cavity resonant peaks increase with increasing CMM dimension. The CMM layer primarily defines the impedance matching condition and so the change in CMM dimension will cause higher impedance mismatch between the CMM and air interface, thereby increasing the reflection at the air-spacer interface with CMM layer and hence reducing the absorption at that particular wavelength. Hence, appropriate design of impedance matched CMM surface is highly desired for perfect absorption.

B. Effect of spacer thickness (*d*)

In order to investigate the effect of absorption spectra with spacer thickness variation, three devices with same CMM dimension, a = 990 nm and varying spacer thickness d = 200, 300, and 400 nm were fabricated. The absorption spectra were measured for these three devices and are shown in Fig. 5. It can be clearly seen that the absorption peak due to cavity resonance shows a significant shift in absorption peak from 1.3 μm to 1.92 μm with a 0.2 μm increase in spacer thickness.

The effect of spacer thickness on cavity resonance can be explained through classical interference theory for electromagnetic waves as follows.[25,53,54] When the electromagnetic wave is incident on the CMM absorber structure, the light is partially reflected from the air-spacer interface with CMM layer and is partially transmitted through the spacer with an initial phase shift. The transmitted wave then propagates through the spacer medium, adding in a phase change of $\beta = n_s k_0 d$, where n_s is the refractive index of the spacer medium, k_0 is the free space wave number and "d" is the spacer thickness. The transmitted wave is then perfectly reflected from the bottom reflector with a π phase shift, after which it gains an additional phase shift of β. Again at the spacer-air interface, partial reflection and transmission takes place. In order to achieve unity absorption, the overall reflection must be zero. Hence, the multiple reflections in the absorber structure must constructively interfere with each other and then the superposition of the multiple reflections must destructively interfere with the direct reflection from the air-spacer interface with CMM, in order to make the overall reflection to be zero.[53]

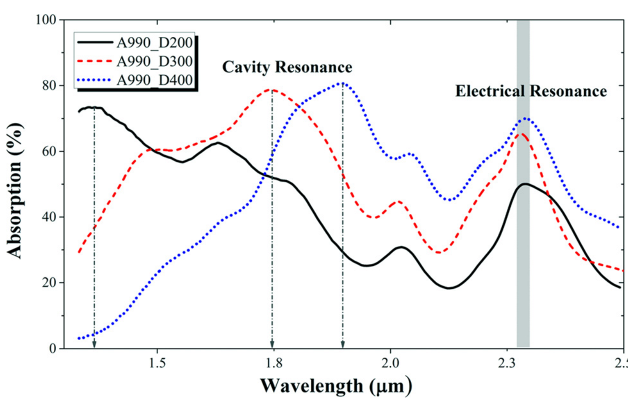

FIG. 5. Measured absorption spectra of three devices with same CMM dimension of $a = 990$ nm and varying SiO_2 thickness of $d = 200$ nm (A990_D200—Black Solid lines), 300 nm (A990_D300—Red Dashed lines), and 400 nm (A990_D400—Blue Dotted lines), respectively.

The spacer thickness plays a key role in the cavity resonant wavelength. Increasing the spacer thickness will cause the increase in phase change (β) and hence the wavelength will red shift to achieve ideal interference condition at the air-spacer interface. Hence, the red shift in cavity resonance peak in the measurement data shown in Fig. 5 follows the prediction made from the above theory. Additionally, the peak absorption intensity for the cavity resonance at different, d values is ~80%. The approximately constant value of peak absorption intensity is due to the fact that CMM dimension remains unchanged in all the three devices, so the surface impedance remains unchanged. Hence, it can be assured that the CMM primarily defines the impedance matching condition to reduce the reflection at the air-CMM interface. It is important to achieve perfect impedance matched condition to attain perfect absorption.[8]

On the other hand, the absorption peak due to the electrical resonance is slightly red shifted with increasing changing spacer thickness as shown in Fig. 5. This can be understood by Eq. (3), as the spacer thickness increases, the current induced in bottom Mo layer decreases thereby reducing the effective bottom Mo inductance, L_2 and so causes a red shift in peak absorption wavelength. Thus, the change in the absorption peak is attributed to the change in effective coupling of electrical resonance in the top CMM and bottom Mo reflector, owing to the increased separation between the CMM and bottom reflector.[55]

IV. DESIGN OF SINGLE BAND ABSORBER

To further investigate the coupling effects between the two resonance mechanisms and to merge both the resonance to achieve single band absorption, 5 devices were designed and fabricated. The electrical resonant peak was fixed around 2.35 μm by retaining the same CMM dimension, $a = 900$ nm and the cavity resonant peak was shifted towards the electrical resonant peak by increasing the SiO_2 spacer thickness from 300 nm to 700 nm in steps of 100 nm. The measured absorption spectra of these 5 devices are shown in Fig. 6. For devices with lower thickness of SiO_2, the two resonances are well separated in wavelength and no significant coupling

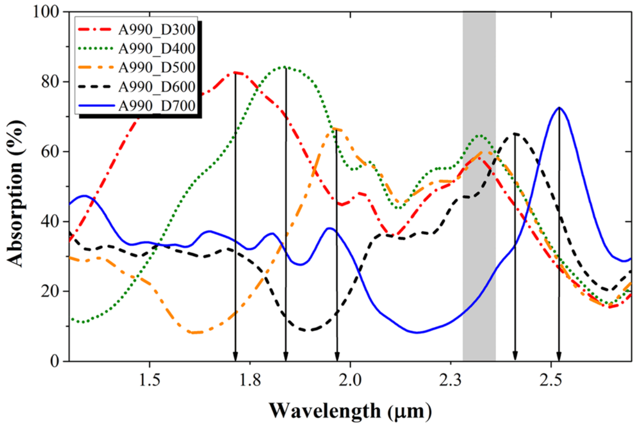

FIG. 6. Measured absorption spectra of five devices with same CMM dimension, a = 990 nm and varying SiO_2 thickness, d = 300 nm (A990_D300—Red Dashed-Dotted lines), 400 nm (A990_D400—Green Dotted lines), 500 nm (A990_D500—Orange Dashed-Dotted-Dotted lines), 600 nm (A990_D600—Black Dashed lines), and 700 nm (A990_D700—Blue Solid lines), respectively.

effect is noticed. As the SiO_2 thickness is increased to $d = 500$ nm, the intensity of cavity resonant peak drops (orange dashed-dotted-dotted curve) and the peak absorption due to electrical resonance shifts towards higher wavelength from 2.35 μm. When $d = 600$ nm (black-dashed curve), the absorption spectra broadens over the wavelength range from 2.1 μm to 2.5 μm, with a distinctive peak at 2.4 μm. Finally at $d = 700$ nm, the electrical and cavity resonance modes merge to provide a single absorption peak at 2.55 μm. More interestingly, the peak absorption wavelength for single band absorber is red shifted from the electrical or cavity resonant peaks which would individually be at 2.35 μm. This can be explained as the effect of hybridization of the two resonant modes at a particular wavelength.[56] The resonant wavelength for the single band absorber (λ_{SBA}), when the electrical and cavity resonances are merged can also be given by Eq. (3). With increasing spacer thickness, the capacitance value of C_2 is decreased and hence the contribution of both capacitances, C_1 and C_2 becomes significant and hence the overall effective capacitance will be higher than the previous case where the resonant frequency is determined majorly by C_1 only. Additionally, the effective inductance of top CMM layer, L_1 is also increased due to increased current induced in the top CMM layer that is caused by the excitation of both resonances at the same wavelength. Hence, the peak absorption wavelength for single band absorber will be shifted to higher wavelengths with increased spacer thickness, compared to the peak absorption due to only electrical or cavity resonance. The cavity resonance was engineered optimally by choosing the appropriate spacer thickness to merge with electrical resonance, because of stronger influence of geometric variation on cavity resonance compared to the electrical resonance. This design methodology has been used and demonstrated for achieving single band absorber from the dual band absorber structure. It is also interesting to note that the Q value of the single band absorber is much higher ~25 compared to the electrical resonance peak (~10) or cavity resonance peak (~5) and can severe for potential applications in infrared detectors.

V. CONCLUSION

In this paper, we report the design and experimental demonstration of a dual band metamaterial absorber, using electrical and cavity resonance mechanisms in near infrared region while adopting a simple trilayer complementary metamaterial absorber structure. The resonant mechanisms are confirmed through a set of experiments by varying the complementary metamaterial dimension and spacer thickness independently. The dual band absorber is then engineered to merge the two resonant mechanisms to be at the same wavelength to achieve single band absorption. The materials - Mo and SiO_2 are CMOS compatible, mass producible and high temperature stable, and so are highly suitable for both commercial and specific rugged applications.

ACKNOWLEDGMENTS

The authors acknowledge the financial support from research grants of A*STAR, SERC Grant Nos. 1021650084 and 1220103064 and AcRF Tier 2 - MOE2012-T2-2-154 at the National University of Singapore.

[1]R. A. Shelby, D. R. Smith, and S. Schultz, "Experimental verification of a negative index of refraction," Science **292**, 77–79 (2001).
[2]J. B. Pendry, D. Schurig, and D. R. Smith, "Controlling electromagnetic fields," Science **312**, 1780–1782 (2006).
[3]D. Schurig, J. J. Mock, B. J. Justice, S. A. Cummer, J. B. Pendry, A. F. Starr, and D. R. Smith, "Metamaterial electromagnetic cloak at microwave frequencies," Science **314**, 977–980 (2006).
[4]N. Fang, H. Lee, C. Sun, and X. Zhang, "Sub–diffraction-limited optical imaging with a silver superlens," Science **308**, 534–537 (2005).
[5]X. Zhang and Z. Liu, "Superlenses to overcome the diffraction limit," Nature Mater. **7**, 435–441 (2008).
[6]B. H. Cheng, Y. C. Lan, and D. P. Tsai, "Breaking optical diffraction limitation using optical hybrid-super-hyperlens with radially polarized light," Opt. Express **21**, 14898–14906 (2013).
[7]Y. T. Wang, B. H. Cheng, Y. Z. Ho, Y. C. Lan, P. G. Luan, and D. P. Tsai, "Gain-assisted hybrid-superlens hyperlens for nano imaging," Opt. Express **20**, 22953–22960 (2012).
[8]N. I. Landy, S. Sajuyigbe, J. J. Mock, D. R. Smith, and W. J. Padilla, "Perfect metamaterial absorber," Phys. Rev. Lett. **100**, 207402 (2008).
[9]H. Tao, N. I. Landy, C. M. Bingham, X. Zhang, R. D. Averitt, and W. J. Padilla, "A metamaterial absorber for the terahertz regime: Design, fabrication, and characterization," Opt. Express **16**, 7181–7188 (2008).
[10]N. Liu, M. Mesch, T. Weiss, M. Hentschel, and H. Giessen, "Infrared perfect absorber and its application as plasmonic sensor," Nano Lett. **10**, 2342–2348 (2010).
[11]J. Hao, L. Zhou, and M. Qiu, "Nearly total absorption of light and heat generation by plasmonic metamaterials," Phys. Rev. B **83**, 165107 (2011).
[12]C. M. Watts, X. Liu, and W. J. Padilla, "Metamaterial electromagnetic wave absorbers," Adv. Mater. **24**, OP98–OP120 (2012).
[13]E. E. Narimanov and A. V. Kildishev, "Optical black hole: Broadband omnidirectional light absorber," Appl. Phys. Lett. **95**, 041106 (2009).
[14]Q. Cheng, T. J. Cui, W. X. Jiang, and B. G. Cai, "An omnidirectional electromagnetic absorber made of metamaterials," New J. Phys. **12**, 063006 (2010).
[15]X. Liu, T. Tyler, T. Starr, A. F. Starr, N. M. Jokerst, and W. J. Padilla, "Taming the blackbody with infrared metamaterials as selective thermal emitters," Phys. Rev. Lett. **107**, 045901 (2011).
[16]J. A. Mason, S. Smith, and D. Wasserman, "Strong absorption and selective thermal emission from a midinfrared metamaterial," Appl. Phys. Lett. **98**, 241105 (2011).
[17]F. Alves, B. Kearney, D. Grbovic, and G. Karunasiri, "Narrowband terahertz emitters using metamaterial films," Opt. Express **20**, 21025–21032 (2012).
[18]T. Maier and H. Bruckl, "Wavelength-tunable microbolometers with metamaterial absorbers," Opt. Lett. **34**, 3012–3014 (2009).

[19]F. B. P. Niesler, J. K. Gansel, S. Fischbach, and M. Wegener, "Metamaterial metal-based bolometers," Appl. Phys. Lett. **100**, 203508 (2012).
[20]F. Alves, D. Grbovic, B. Kearney, and G. Karunasiri, "Microelectromechanical systems bimaterial terahertz sensor with integrated metamaterial absorber," Opt. Lett. **37**, 1886–1888 (2012).
[21]D. Shrekenhamer, W. Xu, S. Venkatesh, D. Schurig, S. Sonkusale, and W. J. Padilla, "Experimental realization of a metamaterial detector focal plane array," Phys. Rev. Lett. **109**, 177401 (2012).
[22]S. B. Mbareka, S. Euphrasiea, T. Barona, L. Thierya, P. Vairaca, B. Cretina, J. P. Guillet, and L. Chusseaub, "Room temperature thermopile THz sensor," Sens. Actuators, A **193**, 155–160 (2013).
[23]Y. Wang, T. Sun, T. Paudel, Y. Zhang, Z. Ren, and K. Kempa, "Metamaterial-plasmonic absorber structure for high efficiency amorphous silicon solar cells," Nano Lett. **12**, 440–445 (2012).
[24]C. Wu, B. Neuner III, J. John, A. Milder, B. Zollars, S. Savoy, and G. J. Shvets, "Metamaterial-based integrated plasmonic absorber/emitter for solar thermo-photovoltaic systems," J. Opt. **14**, 024005 (2012).
[25]J. Sun, L. Liu, G. Dong, and J. Zhou, "An extremely broad band metamaterial absorber based on destructive interference," Opt. Express **19**, 21155–21162 (2011).
[26]T. Chen, S. Li, and H. Sun, "Metamaterials application in sensing," IEEE Sens. J. **12**, 2742–2765 (2012).
[27]H. J. Lee and J. G. Yook, "Biosensing using split-ring resonators at microwave regime," Appl. Phys. Lett. **92**, 254103 (2008).
[28]K. Jaruwongrungsee, W. Withayachumnankul, A. Wisitsoraat, D. Abbott, C. Fumeaux, and A. Tuantranont, "Metamaterial-inspired microfluidic-based sensor for chemical discrimination," in *Proceedings of IEEE Sensors* (2012), pp.1–4.
[29]K. Chen, R. Adato, and H. Altug, "Dual-band perfect absorber for multispectral plasmon-enhanced infrared spectroscopy," ACS Nano **6**, 7998–8006 (2012).
[30]X. Liu, T. Starr, A. F. Starr, and W. J. Padilla, "Infrared spatial and frequency selective metamaterial with near-unity absorbance," Phys. Rev. Lett. **104**, 207403 (2010).
[31]K. Aydin, V. E. Ferry, R. M. Briggs, and H. A. Atwater, "Broadband polarization-independent resonant light absorption using ultrathin plasmonic super absorbers," Nat. Commun. **2**, 517 (2011).
[32]C. W. Cheng, M. N. Abbas, C. W. Chiu, K. T. Lai, M. H. Shih, and Y. C. Chang, "Wide-angle polarization independent infrared broadband absorbers based on metallic multi-sized disk arrays," Opt. Express **20**, 10376–10381 (2012).
[33]B. Y. Zhang, J. Hendrickson, and J. P. Guo, "Multispectral near-perfect metamaterial absorbers using spatially multiplexed plasmon resonance metal square structures," J. Opt. Soc. Am. B. **30**, 656–662 (2013).
[34]P. Bouchon, C. Koechlin, F. Pardo, R. Haïdar, and J. L. Pelouard, "Wideband omnidirectional infrared absorber with a patchwork of plasmonic nanoantennas," Opt. Lett. **37**, 1038–1040 (2012).
[35]S. Q. Chen, H. Cheng, H. F. Yang, J. J. Li, X. Y. Duan, C. Z. Gu, and J. G. Tian, "Polarization insensitive and omnidirectional broadband near perfect planar metamaterial absorber in the near infrared regime," Appl. Phys. Lett. **99**, 253104 (2011).
[36]H. Cheng, S. Chen, H. F. Yang, J. J. Li, X. An, C. Z. Gu, and J. G. Tian, "A polarization insensitive and wide angle dual-band nearly perfect absorber in the infrared regime," J. Opt. **14**, 085102 (2012).
[37]H. M. Lee and J. C. Wu, "A wide-angle dual-band infrared perfect absorber based on metal–dielectric–metal split square-ring and square array," J. Phys. D: Appl. Phys. **45**, 205101 (2012).
[38]J. Hendrickson, J. Guo, B. Zhang, W. Buchwald, and R. Soref, "Wideband perfect light absorber at midwave infrared using multiplexed metal structures," Opt. Lett. **37**, 371–373 (2012).
[39]D. Cheng, J. Xie, H. Zhang, C. Wang, N. Zhang, and L. Deng, "Pantoscopic and polarization-insensitive perfect absorbers in the middle infrared spectrum," J. Opt. Soc. Am. B **29**, 1503–1510 (2012).
[40]N. Zhang, P. Zhou, D. Cheng, X. Weng, J. Xie, and L. Deng, "Dual-band absorption of mid-infrared metamaterial absorber based on distinct dielectric spacing layers," Opt. Lett. **38**, 1125–1127 (2013).
[41]B. Zhang, Y. Zhao, Q. Hao, B. Kiraly, I. C. Khoo, S. Chen, and T. J. Huang, "Polarization-independent dual-band infrared perfect absorber based on a metal-dielectric-metal elliptical nanodisk array," Opt. Express **19**, 15221–15228 (2011).
[42]F. Falcone, T. Lopetegi, M. A. G. Laso, J. D. Baena, J. Bonache, M. Beruete, R. Marques, F. Martın, and M. Sorolla, "Babinet principle applied to the design of metasurfaces and metamaterials," Phys. Rev. Lett. **93**, 197401 (2004).
[43]H. T. Chen, J. F. O'Hara, A. J. Taylor, and R. D. Averitt, "Complementary planar terahertz metamaterials," Opt. Express **15**, 1084–1095 (2007).
[44]C. Rockstuhl, T. Zentgraf, T. P. Meyrath, H. Giessen, and F. Lederer, "Resonances in complementary metamaterials and nanoapertures," Opt. Express **16**, 2080–2090 (2008).
[45]C. Palego, J. Deng, Z. Peng, S. Halder, J. C. M. Hwang, D. Forehand, D. Scarbrough, C. L. Goldsmith, I. Johnston, S. K. Sampath, and A. Datta, "Robustness of RF MEMS capacitive switches with molybdenum membranes," IEEE Trans. Microwave Theory Tech. **57**, 3262 (2009).
[46]C. Goldsmith, D. Forehand, D. Scarbrough, I. Johnston, S. K. Sampath, A. Datta, Z. Peng, C. Palego, and J. C. M. Hwang, "Performance of molybdenum as a mechanical membrane for RF MEMS switches," IEEE MTT-S Int. Microwave Symp. Dig. **2009**, 1229.
[47]B. Ni, X. S. Chen, J. Y. Ding, G. H. Li, and W. Lu, "Impact of resonator rotational symmetry on infrared metamaterial absorber," in *IEEE NUSOD* (2013), pp. 37 and 38.
[48]J. Kischkat, S. Peters, B. Gruska, M. Semtsiv, M. Chashnikova, M. Klinkmüller, O. Fedosenko, S. Machulik, A. Aleksandrova, G. Monastyrskyi, Y. Flores, and W. T. Masselink, "Mid-infrared optical properties of thin films of aluminum oxide, titanium dioxide, silicon dioxide, aluminum nitride, and silicon nitride," Appl. Opt. **51**, 6789–6798 (2012).
[49]M. A. Ordal, R. J. Bell, R. W. Alexander, L. L. Long, Jr., and M. R. Querry, "Optical properties of fourteen metals in the infrared and far infrared: Al, Co, Cu, Au, Fe, Pb, Mo, Ni, Pd, Pt, Ag, Ti, V, and W," Appl. Opt. **24**, 4493–4499 (1985).
[50]J. Zhou, E. N. Economon, T. Koschny, and C. M. Soukoulis, "Unifying approach to left-handed material design," Opt. Lett. **31**, 3620–3622 (2006).
[51]J. Zhou, T. Koschny, and C. M. Soukoulis, "An efficient way to reduce losses of left-handed metamaterials," Opt. Express **16**, 11147–11152 (2008).
[52]Y. Pang, H. Cheng, Y. Zhou, and J. Wang, "Analysis and design of wire-based metamaterial absorbers using equivalent circuit approach," J. Appl. Phys. **113**, 114902 (2013).
[53]H. T. Chen, "Interference theory of metamaterial perfect absorbers," Opt. Express **20**, 7165–7172 (2012).
[54]H. T. Chen, J. Zhou, J. F. O'Hara, F. Chen, A. K. Azad, and A. J. Taylor, "Antireflection coating using metamaterials and identification of its mechanism," Phys. Rev. Lett. **105**, 073901 (2010).
[55]C. Hu, Z. Zhao, X. Chen, and X. Luo, "Realizing near-perfect absorption at visible frequencies," Opt. Express **17**, 11039–11044 (2009).
[56]H. Y. Zheng, X. R. Jin, J. W. Park, Y. H. Lu, J. Y. Rhee, W. H. Jang, H. Cheong, and Y. P. Lee, "Tunable dual-band perfect absorbers based on extraordinary optical transmission and Fabry-Perot cavity resonance," Opt. Express **20**, 24002–24009 (2012).
[57]Z. Liu, C.-Y. Huang, H. Liu, X. Zhang, and C. Lee, "Resonance enhancement of terahertz metamaterials by liquid crystals/indium tin oxide interfaces," Optics Express **21**, 6519–6525 (2013).
[58]Y.-S. Lin, F. Ma, and C. Lee, "Three-dimensional movable metamaterials using electric split-ring resonators," Opt. Lett. **38**, 3126–3128 (2013).
[59]Y.-S. Lin, Y. Qian, F. Ma, Z. Liu, P. Kropelnicki, and C. Lee, "Development of stress-induced curved actuators for a tunable THz filter based on double split ring resonators," Appl. Phys. Lett. **102**, 111908 (2013).
[60]F. Ma, Y. Qian, Y.-S. Lin, H. Liu, X. Zhang, Z. Liu, J. M.-L. Tsai, and C. Lee, "Polarization-sensitive microelectromechanical systems based tunable terahertz metamaterials using three dimensional electric split-ring resonator arrays," Appl. Phys. Lett. **102**, 161912 (2013).
[61]C. P. Ho, P. Pitchappa, P. Kropelnicki, J. Wang, Y. Gu, and C. Lee, "Development of polycrystalline silicon based photonic crystal membrane for mid-infrared applications," IEEE J. Sel. Top. Quantum Electron. **20**, 4900107 (2014).